Integrated Modular Motor Drive Design With GaN Power FETs

Jiyao Wang, *Student Member, IEEE*, Ye Li, *Student Member, IEEE*, and Yehui Han, *Member, IEEE*

***Abstract*—This paper explores the use of GaN power FETs to realize an integrated modular motor drive (IMMD) with an induction motor. A structure in which inverter modules are connected in series is proposed to reduce the module maximum voltages and to offer an opportunity to utilize low-voltage wide-band-gap GaN devices. With the superb switching performance of GaN power FETs, a reduction in IMMD size is achieved by eliminating inverter heat sink and optimizing dc-link capacitors. Gate signals of the IMMD modules are interleaved to suppress the total voltage ripple of dc-link capacitors and to further reduce the capacitor size. Motor winding configurations and their coupling effect are also investigated as a part of the IMMD design. The proposed structure and design methods are verified by experimental results.**

***Index Terms*—Gallium nitride, integration, modular design, motor drives.**

I. Introduction

In applications such as electric vehicles, traction, robotics, and servo motors, it is desirable to reduce the footprint and boost the efficiency of the whole motor and drive system. A conventional drive being used today is placed in a cabinet separated from the electrical motor being driven. Additional cables are required to connect the drive as well as the control and monitor units to the motor. Such kind of design inevitably adds to the volume and weight of the motor drive system and also increases the risks of generating high-voltage transients on the motor windings due to long cable effect. For example, in electrical motors, a critical factor that can shorten a product's service life is the aging of stator winding insulation layers. Cases have been documented in industry when a motor ran well for several years but suddenly failed in a few weeks after installing a variable-frequency drive [1]. The failure is usually due to an overshoot voltage damaging winding insulation layers. The peak voltage on a motor winding when the cable is 1000 ft. ($>$ 300 m) long is more than double the peak voltage on the motor winding when the cable is 30 ft. ($\sim$10 m) long [1]. To ease the overvoltage problem, bulky line reactors or ac filters are often added at the motor input terminals [1].

Manuscript received October 2, 2014; revised December 31, 2014; accepted February 4, 2015. Date of publication March 16, 2015; date of current version July 15, 2015. Paper 2014-IDC-0677.R1, presented at the 2013 IEEE Energy Conversion Congress and Exposition, Denver, CO, USA, September 16–20, and approved for publication in the IEEE Transactions on Industry Applications by the Industrial Drives Committee of the IEEE Industry Applications Society. This work was supported in part by the Grainger Center for Electric Machinery and Electromechanics (CEME) at the University of Illinois and in part by the Wisconsin Electric Machines and Power Electronics Consortium (WEMPEC).

The authors are with the Department of Electrical and Computer Engineering, University of Wisconsin–Madison, Madison, WI 53706 USA (e-mail: jwang229@wisc.edu; lye6@wisc.edu; yehui@engr.wisc.edu).

Color versions of one or more of the figures in this paper are available online at http://ieeexplore.ieee.org.

Digital Object Identifier 10.1109/TIA.2015.2413380

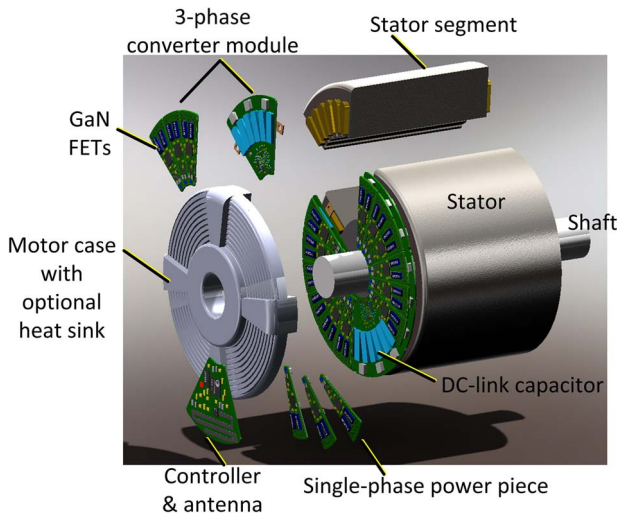

Fig. 1. Three-dimensional illustration of the proposed IMMD.

One of the trends in industry is eliminating the separated drive cabinet and connecting cables to the motor and integrating the motor and the drive as one piece. The motor, the control unit, the communication unit, and protection modules are combined into a single compact package. This new design approach is referred to as "integrated modular motor drives (IMMDs)" in [2] and [3]. As shown in Fig. 1, a drive module consists of an inverter, corresponding gate drivers, a multiple-phase motor winding segment, dc-link capacitors, current and voltage sensors, as well as a communication unit and a microcontroller. The IMMD can further reduce the total system size by sharing the same cooling system between the motor and the drive. Moreover, the IMMD creates a flexible "plug-and-play" capability, i.e., wireless communications are developed enabling intelligent motor performance and functionality. There are a lot of opportunities for IMMD technology, including improvements in the efficiency, power density, and packaging of power electronics. The risks of winding overvoltages in conventional drive systems are also eliminated. It is also possible to simultaneously optimize the motor and drive electronics to increase fault tolerance capacity and minimize drive system cost and complexity for the end users [2], [3].

The physical integration of the motor drive and the machine inside a single housing poses a number of technical challenges. For example, the power electronics have to be designed in such a way that they are able to function successfully in an unfriendly thermal and vibrational environment created by the operating conditions of the machine. Considering relatively high motor operating temperature (90 °C–110 °C for oil cooling), semiconductor devices must have superior efficiency and higher

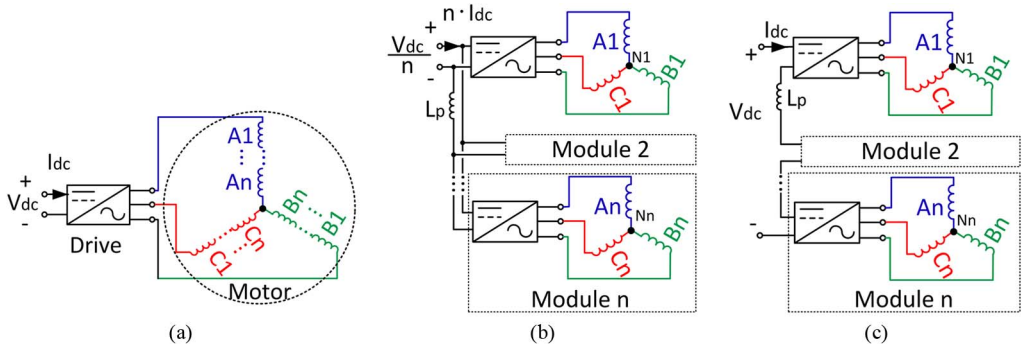

Fig. 2. (a) Conventional motor drive. (b) Conventional IMMD. (c) Proposed structure.

maximum junction temperature than conventional silicon power devices. Wide-band-gap devices such as GaN or SiC may meet these stringent requirements [4], [5]. However, the maximum voltages of most of GaN devices available in the market are less than 200 V, which is too low for many motor drive applications. Even if GaN devices can achieve a maximum voltage of 650 V with a competitive price, the voltage is sill lower than insulated-gate bipolar transistors used in motor control today. In addition, minimizing the total volume and weight associated with the motor drive electronics is one of the biggest challenges faced by IMMD technology available today. Heat sinks and passive components, particularly dc-link capacitors, occupy a large portion of converter volume [2], [3]. For example, bulky capacitors take approximately 30% of the total converter size [6]. These capacitors are the tallest components on the printed circuit board (PCB), and they often determine the overall height of an IMMD. Because the maximum volume of an IMMD is approximated by taking the cross-sectional area of the PCB and multiplying it by the maximum height, the total size of the IMMD is directly proportional to the capacitor height, not just the capacitor volume. Since these capacitors are too tall, it becomes a problem, as shown in [2] and [3], that a traditional IMMD cannot fully integrate all the dc-link capacitors into one package. Moreover, capacitors with large sizes and heights may cause physical vibration when the motor is running. Thus, research has to be directed at identifying power converter architectures or topologies to utilize wide-band-gap devices and to minimize capacitor sizes.

In this paper, an IMMD structure is proposed in which inverter modules are connected in series to reduce the module maximum voltages and to offer an opportunity to utilize low-voltage wide-band-gap GaN devices. The heights and sizes of dc-link capacitors are optimized as a function of switching frequency, and the heat sinks of the IMMD are eliminated. At an even higher power rating, the motor case can also be utilized as an optional heat sink providing extra capability for heat dissipation. In the proposed structure, the choice of capacitor is more flexible because the IMMD module input voltage is a design variable and can be different from the total dc-link input voltage. The total volume of capacitors is reduced through three-phase balanced output power and higher switching frequencies, and interleaving techniques. Moreover, at low voltage levels, there are more choices of different types of capacitors and more flexibility in capacitor selection and optimization. As a result, the dc-link capacitors can be even more flat, and the height of the IMMD is thus reduced.

To utilize GaN FETs to eliminate heat sinks and increase the efficiency of the IMMD, three half-bridge single-phase power pieces are combined into a three-phase converter module to drive a motor segment. The shapes of converter modules match the motor dimensions, and the size of the overall system is minimized. Module voltage is lowered in order to take advantage of 200-V GaN FETs. Although each IMMD module voltage is low, several IMMD modules are connected in series at the input to maintain the total dc-link voltage. The property of motor windings is taken into consideration in order to realize the series-connected IMMD structure. Moreover, IMMD modules can be interleaved to further reduce capacitor size and cost. The controller and communication units are also integrated inside the machine, as shown in Fig. 1.

In Section II, the conventional motor drive structures and the proposed structure are compared side by side. Section III investigates the capacitor volume under different switching frequencies. The sizes of electrolytic and film capacitors in the conventional motor drive and in the proposed IMMD are compared. The gate signal interleaving technique is also discussed. In Section IV, design considerations for GaN power FETs are illustrated. Finally, Section V shows experimental results to validate the proposed design.

II. Proposed IMMD Structure

A. IMMD Structure

In a conventional motor drive, the motor and drive are designed independently, as shown in Fig. 2(a). The drive is usually a two-level inverter with three-phase outputs. This configuration is simple, but it leaves little room to optimize capacitor and semiconductor devices with the motor because the voltage ratings of all components are clamped at the total dc-link voltage. The lack of capacitor choice and the height of available capacitors also make it difficult to integrate the motor drive within the motor.

As discussed in [7]–[9], the machine windings can be split into several segments, and each segment provides a fraction of the total machine voltage, current, and power. These segments can be reconfigured to extend the operating range of the machine. Extra switches and a separated motor drive are needed to drive and reconfigure the machine, but the concepts in [7]–[9]

open the opportunity for using modular motor drives and split winding design for system integration. To further reduce the size of the capacitors and increase the drive power density, an input-parallel structure is presented in [2], [3], [6], and [10], as shown in Fig. 2(b). The motor windings are also split into several segments and combined with converters as IMMD modules. The gate signal interleaving technique is applied to converters in [6] and [10] in order to reduce the total current of dc-link capacitors. In [6] and [10], inverters are two-level full-bridge ones with three-phase outputs. Other multilevel three-phase topologies may be also compatible with the input-parallel structure. The input voltage of one module can be lowered to be a fraction of $V_{\rm dc}$, and as a consequence, semiconductor devices and capacitors can be optimized together with the motor to minimize the height as well as the overall size of the motor drive. The motor windings can be easily altered to accommodate the voltage and current ratings of the motor drive modules. Low-voltage GaN devices can be used in this parallel structure because the input voltage of an inverter module is reduced below the breakdown voltage of GaN devices.

The parallel structure leads to a compromise that the dc-link voltage has to be low and the input current needs to be high. However, in many applications, a low input voltage is difficult to get because the dc-link voltage is usually supplied by a passive rectifier of which the input voltage is fixed and decided by the power grid. In applications where the voltage can be lowered by an extra buck converter or an active rectifier, the overall cost, size, and power loss will also increase. As discussed in [11], the parallel modules may have stability issues during a transient making the parallel structure less appealing for utilizing 200-V GaN devices.

The concepts of multilevel and modular converters, including cascaded H-bridge (CHB) [12], modular multilevel converter (M2C) [13], and modular high-frequency converter (MHF) [14], offer great opportunities to utilize low-voltage devices cascaded to stand a high-voltage input. In these topologies, converter modules are connected in series at inputs or outputs and synthesis single-phase ac output voltages. Modular structures of these converters reduce design complexity and the overall cost of the motor drive system. However, due to the nature of their single-phase structures, converter modules in CHB, M2C, and MHF suffer a fluctuation in output power at twice the motor frequency. DC capacitors at the module inputs are oversized in order to buffer the fluctuating single-phase power. Because of concerns of oversized capacitors, these multilevel topologies are not used for integrated motor drives in this paper.

Fig. 2(c) illustrates the proposed IMMD structure. Three-phase converter modules are series connected at the dc sides and supply their own motor winding segments. Compared to CHB and M2C, the proposed three-phase structure enables constant output power with no fluctuation on dc-link capacitors. The dc-link capacitors are only responsible for the switching ripple. When the switching frequency is increasing, the required capacitance is reduced. The concept behind it is that the motor in the proposed IMMD is not only considered to be a three-phase load but also considered to be magnetic components with electric isolations between different windings. The motor windings can be treated as windings of a rotating transformer that magnetically couple with each other like a primary winding and a secondary winding in a transformer. Different motor windings do not necessarily share the same neutral point potential. Although they are operating at different common voltage potentials, as long as the differential voltage/current on each winding remains the same as in a conventional motor, the magnetomotive force inside the motor, the output torque, and the output power are unaffected. Fig. 2(c) illustrates the proposed IMMD structure where the modules are connected in series at the dc inputs and the motor winding common voltages are biased for different neutral points. The rated voltage of a module is identical to the rated voltage of a module in Fig. 2(b), but the total dc-link voltage is stacked to be the dc-link voltage in Fig. 2(a). There are two approaches of dividing the total dc input voltage equally on the input capacitors of each module: passive balancing or actively balancing. The motor winding segments are identical, the voltages on different drive modules can be passively balanced without any voltage control, which is introduced as the "common duty ratio" method in [15] and [16]. This method is simple, and it is used in the proposed IMMD. When the motor winding segments are not identical and have some parameter variations, for example, in a fault condition, low-frequency voltage ripples will present on dc capacitors of the drive modules. In the latter case, the voltage balance between different modules can be actively regulated using the methods introduced in [17] and [18].

In summary, the proposed IMMD structure has the following advantages.

1) The gate signals of different IMMD modules are interleaved, leading to a size reduction of capacitors for a specified dc-link voltage ripple.
2) Unlike a conventional motor drive, the cost of the IMMD is reduced due to modular design [2].
3) The design is flexible to accommodate different motors. A finished IMMD design can be a combination of structures in Fig. 2(b) and (c). Even when the input dc-link voltage/current is given, there is still some extra room for varying the IMMD module rating voltage/current. This is particularly important in some applications when the dc-link voltage is high and suitable GaN devices are unavailable.
4) The thermal performance is better. Several IMMD modules share the same total power, but semiconductor devices are spread out with larger surface area per volume. The total surface area of semiconductor devices is increased, and the heat is distributed more efficiently over a larger area.
5) Lower IMMD module voltage leads to a lower dv/dt on the motor winding conductor insulation and extends the motor lifespan. The common voltages of the motor windings are a constant value and can be handled by the motor slot insulation. The total cost of motor insulation can thus be reduced compared to a conventional motor drive.
6) The IMMD height is lower, and the IMMD size is small. GaN devices (< 200 V) are used so that IMMD heat sinks are eliminated. When the capacitor maximum voltages are lower, there are more choices of capacitor types and current ratings and more flexibility in capacitor selection and optimization. As a result, the capacitors become more

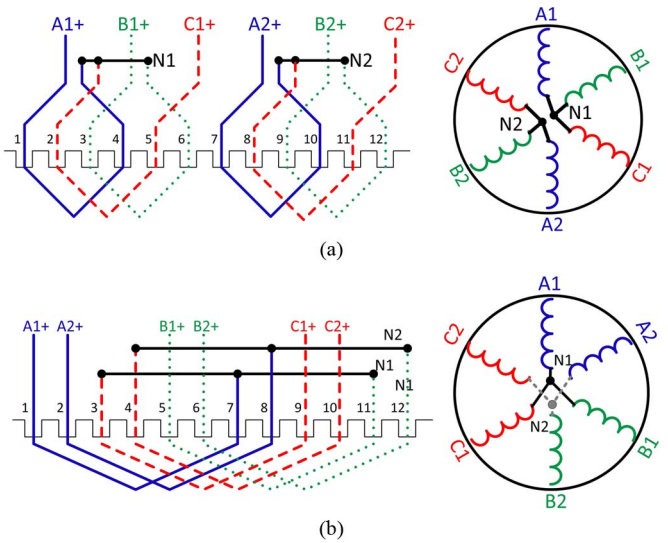

Fig. 3. Split winding configurations. (a) In different poles. (b) In the same pole but different slots.

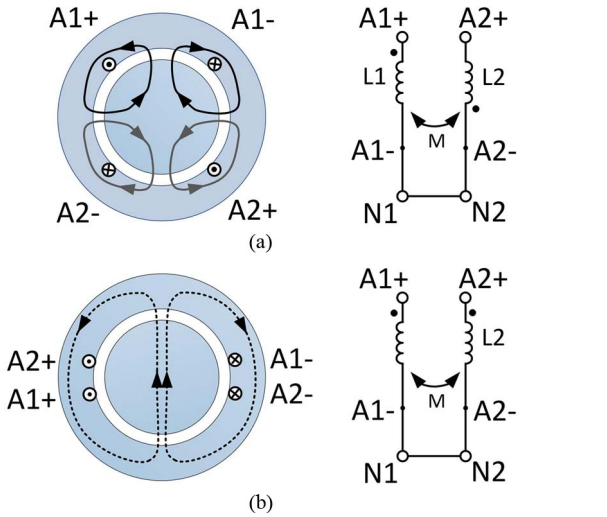

Fig. 4. Equivalent magnetic circuits of winding segments. (a) Winding segments in different poles. (b) Winding segments in the same pole but different slots.

flat and less tall on the PCB, and the maximum height of the IMMD is thus reduced.

7) The proposed IMMD can match with a multilevel front-end rectifier design that inherently has several capacitors connected in series [19].

B. Winding Configurations

The converter module requires motor windings to be separated into multiple parts. The approach to split the motor is straightforward: winding coils do not need to be interconnected with each other as in a conventional motor. Instead, coils in different pole pairs/slots can be directly connected to different IMMD modules. By this approach, the motor property remains identical as in the original motor design. Meanwhile, the complicated interconnections between coils are avoided, and consequently, the manufacturing process is simplified, and the motor cost is reduced.

For the sake of simplification, two fundamental winding configurations are introduced: 1) coils in different pole pairs and 2) distributed winding coils in the same pole pair and the same phase, but in different slots. A real motor winding configuration is usually a combination of these two fundamental configurations. To clearly identify these two fundamental winding configurations, simplified examples are presented in Fig. 3. Fig. 3(a) illustrates a three-phase, four-pole, and 12-slot motor (one slot per pole per phase). The winding coils in different pole pairs are split into two segments. The two winding segments could be connected in series or in parallel in a conventional motor, so they share the same output terminals. However, for an IMMD design, the windings in different pole pairs are separated and have their own neutral points N1 and N2 as well as output terminals A1 and A2. This configuration does not change any motor electrical property or induce extra cost but provides more flexibility to match the property of the IMMD.

The second fundamental configuration is shown in Fig. 3(b). The distributed lap-winding coils in a three-phase, two-pole, and 12-slot motor (two slots per pole per phase) is split into two segments. They should be series connected in a conventional motor to form a lap-winding configuration. In an IMMD design, the winding coils in two adjacent slots are completely separated and can be controlled individually.

In an IMMD design, these two configurations can be combined into a more complicated one. For example, a motor with four poles and two slots per pole per phase could be split into four winding segments. Two segments are split, as shown in Fig. 3(a), and the other two are split, as shown in Fig. 3(b). These configurations also open the opportunity for controlling motor in a more refined way [3].

C. Motor Winding Coupling Effect

The winding segments are actually magnetically coupled with each other. The two fundamental configurations introduced in Fig. 3 have different magnetic properties. Fig. 4(a) shows the corresponding magnetic equivalent circuit of the motor in Fig. 3(a). Two winding segments A1 and A2 are in different poles and have $M<0$. The absolute value of M represents the coupling factor of two windings, and the sign of M represents the dots of coupling. If the rotor center shaft is not magnetizing, which is usually the case, the coupling factor will be close to zero. The different poles in a motor are all connected to the same rotor shaft; thus, they are equivalent to different motors attached to the same line shaft. The control method of line-shaft motors can be found in [20].

Fig. 4(b) shows the case of Fig. 3(b). Since the winding branches are in the same phase and same pole, α (electrical angle between two windings) is less than 90°. Assume air-gap length, rotor diameter, and motor length are g, D, and L, respectively. M could be calculated as

$$M = \left(1 - \frac{2\alpha}{\pi}\right) DL \frac{\mu_0 N_{A1} N_{A2}}{2g} > 0. \tag{1}$$

When the phase shift angle α becomes smaller, the coupling is stronger. With a gate signal interleaving technique, the magnetic coupling between segments will influence the output line

current ripple. According to [21], $M < 0$ results in smaller line current ripple, and $M > 0$ has larger line current ripple compared to the line current ripple when $M = 0$. These two configurations can both be driven by IMMD modules. The $M < 0$ case will reduce the line current ripple. For the $M > 0$ case, although the line current ripple is increased, the effect is negligible because the motor line inductance is more than enough to limit the current ripple under high-frequency pulsewidth modulation (PWM). In addition, the total flux ripple is smaller if gate signal interleaving is applied, resulting in a smaller motor magnetic loss caused by PWM.

III. Capacitor Volume Evaluation

A. Capacitor Volume Versus Switching Frequency

Since the capacitors play a dominant role in reducing the IMMD volume, it is necessary to compare the capacitor size between a conventional motor drive and an IMMD. In this section, the switching frequency of the motor drive ranges from 10 to 40 kHz.

Before evaluating the capacitor volume, an important observation should be emphasized first: Electrolytic capacitor size is limited by the capacitor rating current (RMS value) and not by the capacitance. This is because electrolytic capacitors usually have very large capacitance but small current rating. In other words, if an electrolytic capacitor is selected such that the current rating meets the requirement, its capacitance is far more than necessary. Following the design procedure in [22], the dc-link capacitor must satisfy the worst case current, and the capacitor RMS current value of a three-phase inverter can be calculated by (2) as derived in [22], i.e.,

$$\begin{aligned} I_{\mathrm{Cap\_RMS_{max}}} &= I_{\mathrm{Line\_RMS}} \sqrt{2\mathrm{m}\left[\frac{\sqrt{3}}{4\pi} + \cos^2\Phi\left(\frac{\sqrt{3}}{\pi} - \frac{9}{16}\mathrm{m}\right)\right]}_{\max} \\ &\approx 0.65\, I_{\mathrm{Line\_RMS}} \\ \mathrm{m} &= \frac{\widehat{V}_{\mathrm{out}}}{0.5\mathrm{V_{dc}}} \qquad \mathrm{m} \in \left[0, \frac{2}{\sqrt{3}}\right] \end{aligned} \tag{2}$$

where m is the modulation index defined as the peak amplitude of the output voltage divided by half the dc-link voltage, and $\cos\,\Phi$ is the power factor. The maximum value is reached when $\mathrm{m} = 0.6$ and $\cos\Phi = 1.0$ [22].

At a higher switching frequency, the dc-link capacitor RMS current does not change, which means that the size of an electrolytic capacitor does not depend on the switching frequency. Two simulation models can further illustrate this phenomenon. They simulate the currents and voltages of a two-level three-phase converter module, as shown in Fig. 5. A closed-loop dq-axis current proportional–integral controller is used to regulate the line currents. The input current ripple Δi_{dc} is proportional to the voltage ripple amplitude Δv_{dc} and inversely proportional to the filter inductor L_p and the switching frequency. The filter inductor L_p in the simulation is large enough such that the input current ripple Δi_{dc} from the voltage source is negligible compared to the current ripples into the capacitor. As a result, the switching ripple from the converter is fully handled by the dc-link capacitor. These two models have identical input and output voltage, current, and power. The only difference is the switching frequency: 20 and 40 kHz for each model, as shown in Figs. 6 and 7, respectively. Fig. 8 shows in the zoom-in ripples near the peak of the line current waveforms.

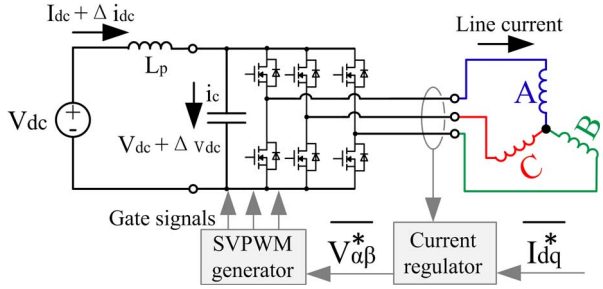

Fig. 5. Simulation model of one IMMD module.

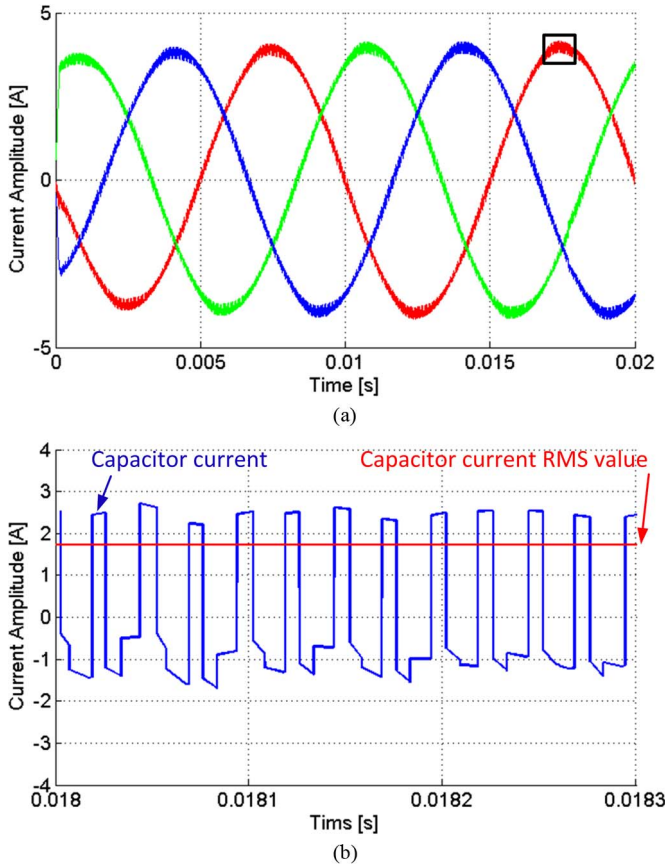

Fig. 6. IMMD with a 20-kHz switching frequency. (a) Output line current waveform. (b) DC-link capacitor current with a 1.80-A RMS value.

From the simulation results, although the frequency of dc-link capacitor ripple current is in accordance with the switching frequency, the RMS value of dc-link ripple current does not change. If an electrolytic capacitor is selected for the 20-kHz model, when the switching frequency increases to 40 kHz, the electrolytic capacitor size cannot be reduced since the RMS current remains the same. Table I summarizes the electrolytic capacitor selection for 10-, 20-, and 40-kHz models.

From [23], the dc-link input usually has a 1% maximum voltage ripple requirement. Because the electrolytic capacitor selection is based on the RMS current rating, the capacitance is much larger than necessary for the voltage ripple requirement,

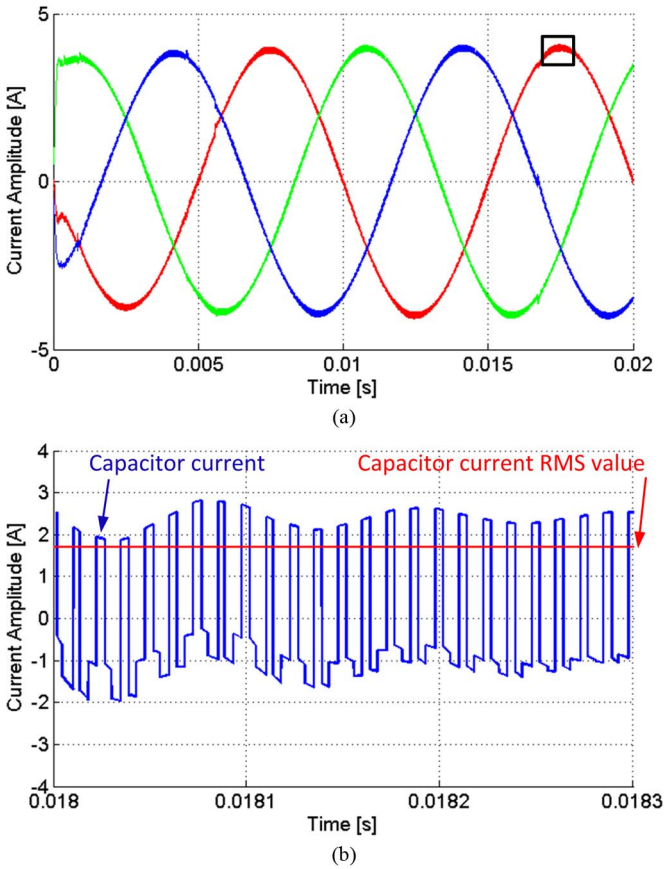

Fig. 7. IMMD with a 40-kHz switching frequency. (a) Output line current waveform. (b) DC-link capacitor current with a 1.78-A RMS value.

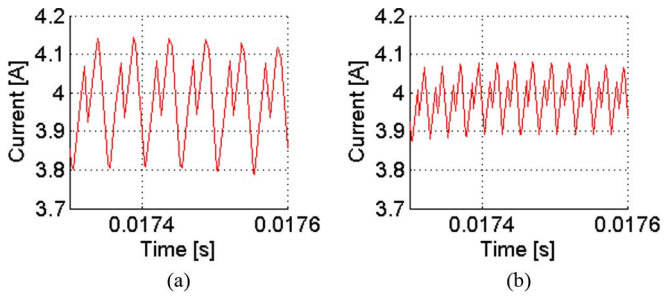

Fig. 8. Line current ripples zoomed in at (a) 20 kHz and (b) 40 kHz.

as illustrated in Table I. In contrast, film capacitors and ceramic capacitors have much smaller capacitance per volume than electrolytic capacitors, but have a larger RMS current rating. These capacitors are selected according to the maximum voltage ripple requirement instead of the maximum current ripple requirement. When the switching frequency increases, required capacitance can be smaller, and the capacitor size can be reduced. Table I also shows the selection of film capacitors. A single film capacitor of 80, 40, or 20 μF is acceptable, but it is more desirable to parallel several 10-μF film capacitors on the PCB. Although the total capacitance remains identical compare to a single film capacitor, the 10 μF ones are more flat and lead to a smaller IMMD volume. From the comparison, film capacitors have a better performance than electrolytic capacitors in terms of size when the frequency is beyond 20 kHz. Moreover, film capacitors also have other advantages over electrolytic capacitors such as better thermal performance, making them appealing to motor drive applications [24], [25]. As the switching frequency increases, the capacitance is reduced, and the capacitor RMS current rating goes down. It will hit an optimal point of capacitor selection when the RMS current rating of capacitors drops to the RMS current value of the IMMD module. Further increasing the switching frequency can no longer reduce the capacitor size. In the example shown in Table I, the optimal frequency for film capacitors is around 108 kHz, and at this frequency, the total size of film capacitors is smaller than electrolytic capacitors (see Fig. 9).

TABLE I
CAPACITOR SELECTION FOR 200-V IMMD MODULES

	Switching frequency	10 kHz	20 kHz	40 kHz
Electrolytic capacitor	Capacitor RMS current in Fig. 6(b) & Fig. 7(b)	1.86 A	1.80 A	1.78 A
	Max. voltage ripple limit	2 V	2 V	2 V
	Minimum capacitance needed	80 µF	39 µF	19 µF
	Electrolytic cap. type	250 V Panasonic EETXB2E821KJ		
	Capacitance	820 µF		
	RMS current rating	2.0 A		
	Volume	35325 mm^3		
	Voltage ripple on capacitor	0.019 V	0.09 V	0.046 V
Film capacitor	Film capacitor type	250V EPCOS 8 * B32524	250V EPCOS 4 * B32524	250V EPCOS 2 * B32524
	Capacitance	80 µF	40 µF	20 µF
	RMS current rating	21.6 A	10.8 A	5.4 A
	Volume	67724 mm^3	33862 mm^3	16931 mm^3
	Voltage ripple on capacitor	2 V	2 V	2 V

For low-power and low-vibration applications, ceramic capacitors are also promising candidates because of their compact sizes. The performance of ceramic capacitors is similar to film capacitors.

B. Gate Signal Interleaving Technique

The function of dc-link capacitors is to stabilize the dc-link voltage and to smoothen the input current from a dc source [6]. The total dc-link voltage ripple needs to meet the 1% requirement as discussed in [23]. The purpose of interleaving

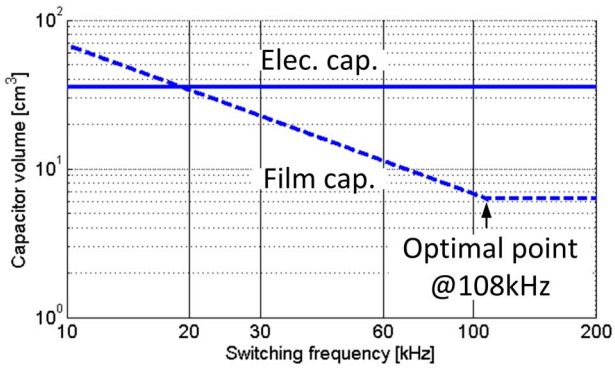

Fig. 9. Total volumes of electrolytic and film capacitors for a 200-V 2.0-A IMMD module under different switching frequencies.

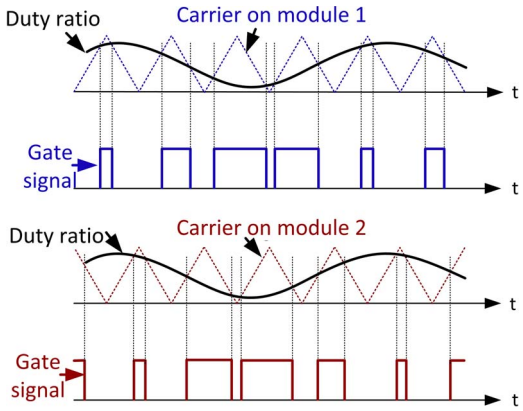

Fig. 10. Illustration of 180° gate signal interleaving.

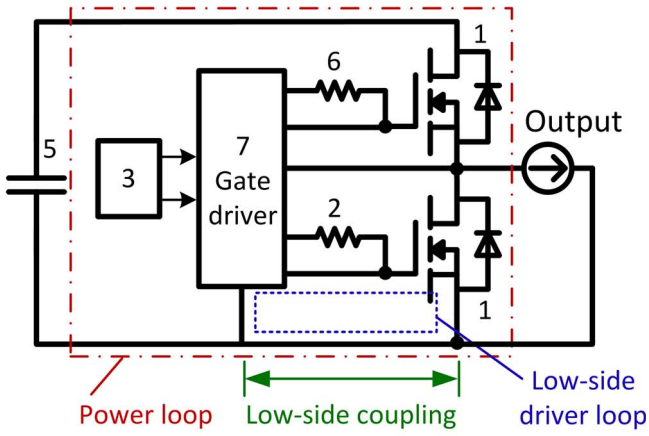

(a)

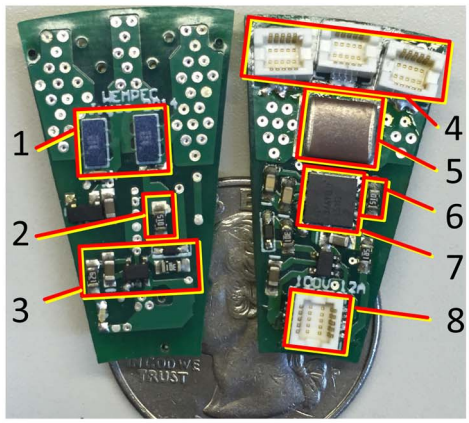

(b)

Fig. 11. (a) Schematic and (b) photo of a single-phase half-bridge module: 1, GaN FETs; 2, low-side turn-on resister; 3, deadtime generator; 4, power connectors; 5, dc capacitors, 6, high-side turn-on resistor; 7, gate driver; 8, signal connector.

gate signals is to build IMMD modules with even smaller capacitors. To achieve this, the gate signals of different IMMD modules are shifted from each other. Since they still have identical duty ratios, the output sinusoidal voltages at the fundamental frequency are the same. However, the shifted gate signals will create shifted current/voltage ripples, Thus, when the ripples are combined, they tend to cancel each other and result in a smaller total ripple voltage on the dc link. A similar interleaving mechanism is also effective for space vector PWM (SVPWM). For example, active switching vectors for two modules alternate at a half-switching cycle difference, resulting in ripples shifted by 180°. In this way, the module can use smaller capacitors. Although the voltage ripple on one module is larger than the 1% requirement, when several modules are working simultaneously, the total dc-link ripple still meets the 1% requirement, and the capacitor size is smaller than the case without interleaving. Fig. 10 shows an example of two IMMD modules with gate signal interleaving. Module PWM carriers and gate signals are shifted by 180°. This interleaving technique reduces the voltage ripple requirement on each module, but it does not reduce the capacitor current.

In the proposed IMMD structure, all the modules are connected in series. The dc-link voltages of the modules are constant values with 1% ripples. They will be synthesized, and the ripples tend to get diminished by each other, resulting in smaller total dc-link voltage ripple amplitude. In addition, the frequency of total voltage ripple is also doubled because of interleaving, making it possible for further reduction of the input filter size.

TABLE II
LOOP LENGTHS AND FEA INDUCTANCES

	Power	Driver	Coupling
Loop length [mm]	23.2	8.9	1.6
Inductance [nH]	3.97	1.73	0.107

IV. DESIGN CONSIDERATIONS FOR GAN POWER FETS

As discussed in [26], the switching loop inductance of a GaN FET is an important design parameter. To improve the switching performance, the parasitic inductances in a power loop and a gate driver loop should both be minimized. In addition, the coupling between these two loops should be as small as possible; otherwise, the power loop will have a negative influence on the gating signal. Fig. 11 shows the schematic and design of a half-bridge power inverter. The lengths of the power loop and driver loop are designed as short as possible, so that the coupling between these two loops is negligible. Table II presents the finite-element analysis (FEA) results of the parasitic values of these three loops.

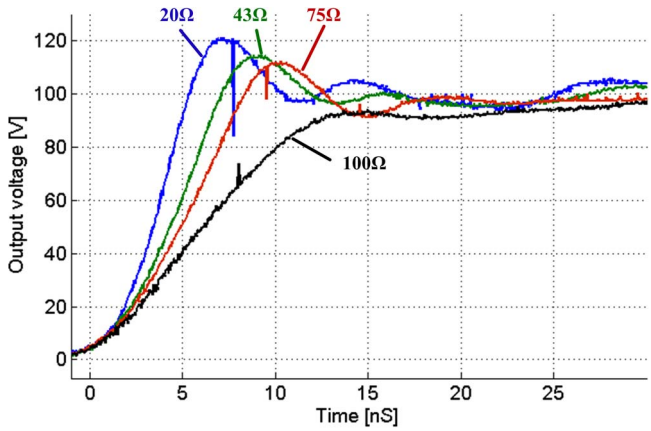

Fig. 12. Switching waveforms for different turn-on resistances.

TABLE III
SWITCHING PERFORMANCE AT 100 kHz, 5 A

Extra Gate res. For turn-on [Ω]	20	43	75	100
Rise time [nS]	4.3	5.6	8.9	10.8
Overshoot [%]	21.3	14	6.6	0
Switching loss [W]	0.22	0.28	0.45	0.54

The extra gate resistance for turning on a GaN FET is also a factor that influences the performance of an inverter. Fig. 12 shows the rising edge of the output voltage of a phase leg, which is dominated by the extra resistance connected with the gate for turning on the high-side switch. Smaller resistance for turn-on leads to a faster rising edge but a larger overshoot. As a consequence, the switching loss is lower, but the device voltage stress is larger. A practical choice in this case would be around 50 Ω, resulting in a small overshoot and an acceptable switching loss (see Table III).

V. EXPERIMENTAL RESULTS

Fig. 13 shows an integrated modular motor drive inside a commercial induction motor. The drive is implemented with two inverter modules connected in series using the structure presented in Fig. 2(c). The drive, its dc-link capacitors, sensors, as well as the controller board are all installed in the space between the housing and the winding, and no extra space and interconnect cables are needed outside of the motor. The total footprint of the motor and drive system has been reduced to the footprint of the original motor. The motor is a 24-slot two-pole induction motor reconfigured to six leads. The original concentric short-pitched windings can be split into two halves quite conveniently by its nature without changing any motor property. Two inverter modules implemented with EPC GaN devices match the physical size of the motor. The IMMD uses an open-loop V/f control with SVPWM. Fig. 13 shows some photos of the prototype IMMD.

Table IV shows the design specifications of the inverters. The module input capacitance needs to be at least 40 μF to fulfill the 1% voltage ripple requirement according to simulation results. It is decided to use 50-μF capacitance in total in the hardware. Inverter modules with EPC GaN FETs are distributed

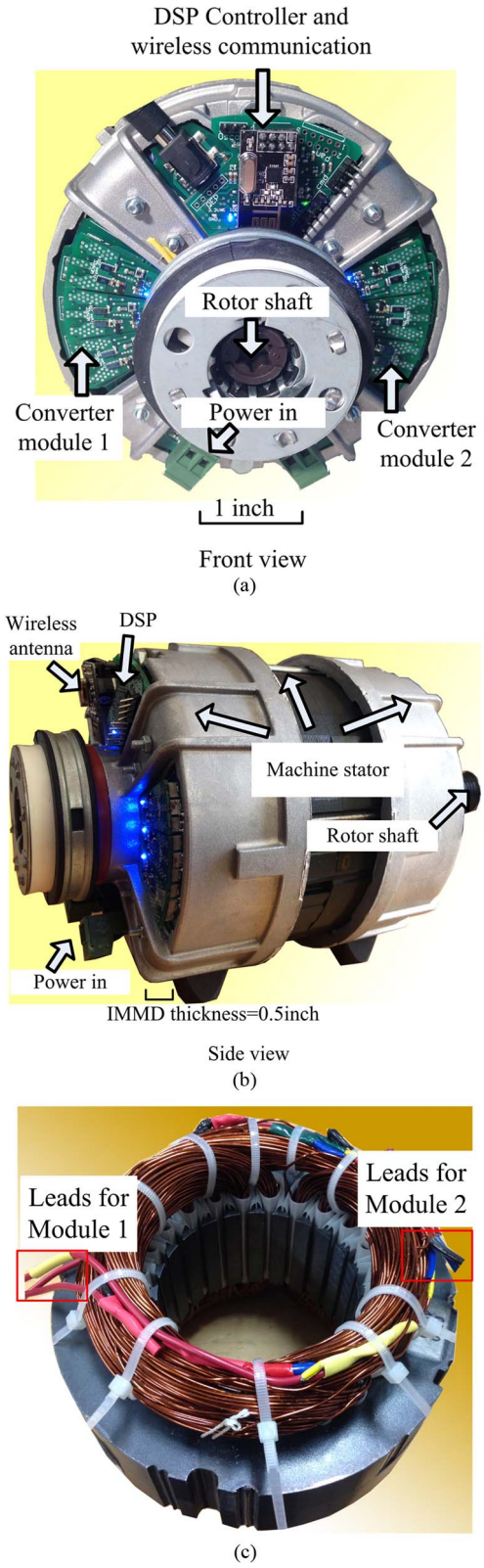

Fig. 13. Prototype IMMD. (a) Front view. (b) Side view. (c) Rewound motor stator core.

along the circumference of the motor, resulting in a large area for heat dissipation. The power rating of this tested motor is relatively small; thus, the motor temperature is within limit. If the power rating increases, thermal design has to be taken into

TABLE IV
PROTOTYPE IMMD SPECIFICATIONS

Total dc-link voltage	200 [V]
Number of modules	2
Module voltage	100 [V]
Module capacitance	50 [μF]
GaN FETs	EPC2018
FET maximum current	12 [A peak]
Switching frequency	100 [kHz]
Motor type	3 phase induction motor
Number of poles	2
Motor # slots	36
Motor winding	1 layer, short pitched, concentric
Motor line voltage	190 [V]
Motor line current	5 [A rms]

consideration. Air holes can be added on the PCB or on the side of the motor case to boost air venting. Moreover, extra heat sinks can be installed between semiconductor devices and the motor, with vents installed on the side of the motor for air cooling [2] or pipes for oil or water cooling [6]. The controller and communication devices are also integrated inside the motor, as shown in Fig. 13(a) and (b). The motor communicates with the user via a 2.4-GHz wireless transceiver. The wireless remote controller can program the IMMD to start, stop, reverse, and accelerate the motor. This wireless communication will be an interface for improving intelligent motor performance and functionality in the future.

The experimental results in Fig. 14(a) illustrate the operation of the prototype IMMD and validate that the proposed IMMD can share voltage equally among different modules in a passive balancing approach. In a full operation cycle, the motor is first accelerating to the command speed and then keeps a constant speed for about 1 s, and finally, it slows down. During the whole cycle, the module voltage remains at 100 V, which is half of the total dc-link voltage. Fig. 14(b) presents the details of the voltage ripple on both modules. Fig. 14(c) shows the three-phase currents in steady state from one module during operation. Fig. 14(d) shows the thermal performance of the IMMD under the load condition of Fig. 14(c). The picture was taken after the motor ran for 30 min and the temperatures of the IMMD and motor were stable. To illustrate the interleaving technique, dc-link voltage ripple should be examined. However, the dc-link voltage ripple is too small to be measured accurately. In the experiment, to illustrate the interleaving in a better way, dc-link input current is measured to indicate the voltage ripple. The switching frequency is reduced to 20 kHz to get a larger current ripple. As shown in Fig. 14(e), the current ripple on account of interleaving is much smaller than that in the case of non-interleaving. Meanwhile, the ripple frequency is almost double for interleaving design. These experimental results validate the proposed IMMD design and show the ability of the IMMD to operate as a conventional motor drive.

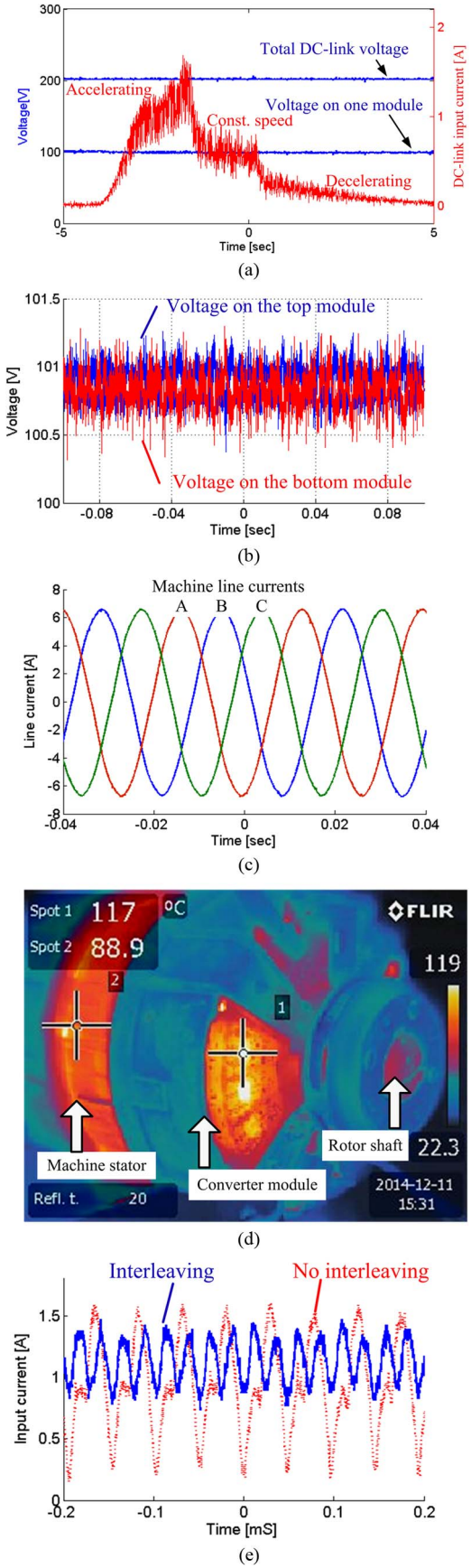

Fig. 14. Experimental results. (a) Full cycle of the motor. (b) Voltage balancing on two modules. (c) Three-phase currents from one IMMD module during a normal operation. (d) Thermal performance. (e) DC-link input current with and without interleaving.

VI. Conclusion

The magnetic properties of motor windings are utilized to benefit the IMMD design. Two fundamental winding configurations are discussed in this paper, and they can be applied in an IMMD with a compact design. Modular converters with GaN FETs are proposed to eliminate heat sinks and provide superior switching performance. With a high switching frequency, the size and height of capacitors are reduced, and all the capacitors can be integrated into the IMMD. In this paper, an approach has been developed to evaluate the capacitor size and to find the optimal point in the capacitor selection. In addition, gate signals are interleaved to further reduce the size of capacitors. With the techniques introduced in this paper, a fully functional plug-and-play IMMD prototype is integrated into a 36-slot, 190-V, 5-A induction motor. The proposed IMMD structure has been proved to be feasible through experimental results.

References

[1] "YASKAWA application report: Long drive/motor leads," Yaskawa Elect. Amer., Inc., Kitakyushu, Japan, Rep. AR.AFD.05, 2006.

[2] N. R. Brown, T. M. Jahns, and R. D. Lorenz, "Power converter design for an integrated modular motor drive," in *Conf. Rec. IEEE IAS Annu. Meeting*, 2007, pp. 1322–1328.

[3] B. J. Sykora, "Development of a demonstrator model of an integrated modular motor drive," M.S. thesis, Dept. Elect. Comput. Eng., Univ. Wisconsin, Madison, WI, USA, 2008.

[4] T. Morita *et al.*, "99.3% efficiency of three-phase inverter for motor drive using GaN-based gate injection transistors," in *Proc. IEEE Appl. Power Electron. Conf.*, 2011, pp. 481–484.

[5] D. Ueda *et al.*, "Present and future prospects of GaN-Based power electronics," in *Proc. 9th Int. Conf. Solid-State Integrated-Circuit Technol.*, 2008, pp. 1078–1081.

[6] G. Su and L. Tang, "A segmented traction drive system with a small DC bus capacitor," in *Proc. IEEE Energy Convers. Congr. Expo.*, 2012, pp. 2847–2853.

[7] E. Nipp, "Alternative to field-weakening of surface-mounted permanent-magnet motors for variable-speed drives," in *Conf. Rec. IEEE IAS Annu. Meeting*, 1995, pp. 191–198.

[8] T. Gerrits, C. G. E. Wijnands, J. J. H. Paulides, and J. L. Duarte, "Dynamic machine operation transitions," in *Proc. IEEE Veh. Power Propulsion Conf.*, 2013, pp. 1–6.

[9] H. Hijikata and K. Akatsu, "Design and online winding reconfigurations method of matrix motor," in *Proc. IEEE Energy Convers. Congr. Expo.*, 2012, pp. 1300–1337.

[10] S. C. Tang, D. M. Otten, T. A. Keim, and D. J. Perreault, "Design and evaluation of a 42-V automotive alternator with integrated switched-mode rectifier," *IEEE Trans. Energy Convers.*, vol. 25, no. 4, pp. 983–992, Aug. 2010.

[11] C. E. Jones, M. Barnes, and A. J. Forsyth, "Stability analysis of motor drive interactions in aircraft electrical systems," in *Proc. 14th Eur. Conf. Power Electron. Appl.*, 2011, pp. 1–10.

[12] P. W. Hammond, "A new approach to enhance power quality for medium voltage AC drives," *IEEE Trans. Ind. Appl.*, vol. 33, no. 1, pp. 202–208, Jan./Feb. 1997.

[13] M. Glinka and R. Marquardt, "A new AC/AC multilevel converter family," *IEEE Trans. Ind. Electron.*, vol. 52, no. 3, pp. 662–669, Jun. 2005.

[14] L. Lambertz, R. Marquardt, and A. Mayer, "Modular converter systems for vehicle applications," in *Proc. Emobility—Elect. Power Train*, 2010, pp. 1–6.

[15] J. Shi, J. Luo, and X. He, "Common-duty-ratio control of input-series output-parallel connected phase-shift full-bridge DC–DC converter modules," *IEEE Trans. Power Electron.*, vol. 26, no. 11, pp. 3318–3329, Nov. 2011.

[16] R. Giri, V. Choudhary, R. Ayyanar, and N. Mohan, "Common-duty-ratio control of input-series connected modular DC–DC converters with active input voltage and load-currents haring," *IEEE Trans. Ind. Appl.*, vol. 42, no. 4, pp. 1101–1111, Jul./Aug. 2006.

[17] J. W. Kimball, J. T. Mossoba, and P. T. Krein, "A stabilizing, high-performance controller for input series-output parallel converters," *IEEE Trans. Power Electron.*, vol. 23, no. 3, pp. 1416–1427, May 2008.

[18] L. Tarisciotti *et al.*, "Active DC voltage balancing PWM technique for high-power cascaded multilevel converters," *IEEE Trans. Ind. Electron.*, vol. 61, no. 11, pp. 6157–6167, Feb. 2014.

[19] C. Klumpner, F. Blaabjerg, and P. Thogersen, "Evaluation of the converter topologies suited for integrated motor drives," in *Conf. Rec. IEEE IAS Annu. Meeting*, 2003, pp. 890–897.

[20] M. A. Valenzuela and R. D. Lorenz, "Electronic line-shafting control of paper motor drives," in *Proc. Pulp Paper Ind. Technol. Conf.*, 2000, pp. 106–112.

[21] L. Wong, P. Xu, P. Yang, and F. C. Lee, "Performance improvements of interleaving VRMs with coupling inductors pit," *IEEE Trans. Power Electron.*, vol. 16, no. 4, pp. 499–507, Jul. 2001.

[22] J. W. Kolar and S. D. Round, "Analytical calculation of the RMS current stress on the DC link capacitor of voltage DC link PWM converter systems," *Proc. Inst. Elect. Eng.—Elect. Power Appl.*, vol. 153, no. 4, pp. 535–543, Jul. 2006.

[23] M. Salcone and J. Bond, "Selecting film bus link capacitors for high performance inverter applications," in *Proc. IEEE Int. Electric Mach. Drives Conf.*, 2009, pp. 1692–1699.

[24] R. Maheshwari, S. Munk-Nielsen, and K. Lu, "An active damping technique for small DC-link capacitor based drive system," *IEEE Trans. Ind. Informat.*, vol. 9, no. 2, pp. 848–858, Oct. 2013.

[25] M. Hinkkanen and J. Luomi, "Induction motor drives equipped with diode rectifier and small DC-link capacitance," *IEEE Trans. Ind. Electron.*, vol. 55, no. 1, pp. 312–320, Jan. 2008.

[26] D. Reusch, D. Gilham, Y. Su, and F. C. Lee, "Gallium nitride based 3D integrated non-isolated point of load module," in *Proc. IEEE Appl. Power Electron. Conf. Expo.*, 2012, pp. 38–45.

Jiyao Wang (S'11) received the B.S. degree in electrical engineering from Tsinghua University, Beijing, China, in 2010 and the M.S. degree in electrical and computer engineering from the University of Wisconsin-Madison, Madison, WI, USA, in 2012. He is currently working toward the Ph.D. degree at the University of Wisconsin-Madison.

His research interests include motor drives, motor control, and multilevel converters.

Ye Li (S'13) received the B.S. degree in electrical engineering from Tsinghua University, Beijing, China, in 2001 and the M.S. degree in electrical engineering from the University of Wisconsin–Madison, Madison, WI, USA, in 2014. He is currently working toward the Ph.D. degree in electrical engineering at the University of Wisconsin–Madison.

He is currently a Research Assistant with the Department of Electrical and Computer Engineering, University of Wisconsin–Madison, and is affiliated with the Wisconsin Electric Machines and Power Electronics Consortium (WEMPEC). His primary research interests are power electronics and applications in energy storage systems, motor drive systems, and renewable energy systems.

Yehui Han (S'04–M'10) received the B.S. and M.S. degrees from Tsinghua University, Beijing, China, in 2000 and 2003, respectively, and the Ph.D. degree from the Massachusetts Institute of Technology, Cambridge, MA, USA, in 2010, all in electrical engineering.

He is currently an Assistant Professor with the Department of Electrical and Computer Engineering, University of Wisconsin–Madison, Madison, WI, USA, and is affiliated with the Wisconsin Electric Machines and Power Electronics Consortium (WEMPEC). His primary research interests are power electronics and applications in renewable energy and energy efficiency.

Dr. Han was a recipient of the MIT Landsman Fellowship and four IEEE Prize Paper Awards.